On the correlative microscopy analyses of nano-twinned domains in 2 mol% zirconia alloyed yttrium tantalate thermal barrier material

K. Gururaj, Mainak Saha, Sumit Kumar Maurya, Rajat Nama, A. Alankar, M.B. Ponnuchamy, K.G. Pradeep

On the correlative microscopy analyses of nano-twinned domains in 2 mol% zirconia alloyed yttrium tantalate thermal barrier material

K. Gururaj[1], Mainak Saha[1], Sumit Kumar Maurya[2,3], Rajat Nama[1], A. Alankar[2], M. B. Ponnuchamy[1], K. G. Pradeep[1]

[1]Correlative Microscopy Laboratory, Department of Metallurgical and Materials Engineering, Indian Institute of Technology Madras, Chennai – 600036

[2]Department of Mechanical Engineering, Indian Institute of Technology Bombay, Mumbai – 400076.

[3]Department of Materials Science and Engineering, Monash University, Victoria 3800, Australia

Abstract

Formation of nano-twinned domains associated with ferro-elastic transformation in 2 mol.% ZrO_2 alloyed $YTaO_4$ has been investigated using a correlative microscopy approach. Transmission Kikuchi diffraction reveals the presence of two phases, monoclinic (M) and tetragonal (T) in the material sintered at 1485 °C for 3 hr. The microstructure comprises of alternate nano-twinned domains with an average spacing of 154.07 ± 42.52 nm. Crystallographic symmetry based spontaneous strain analyses support the observation of single domain state. Ab-initio calculations further indicate the propensity of stabilizing both M and T phases at room temperature as a function of ZrO_2 alloying, without any change in chemical composition, as is evidenced by atom probe tomography.

Key words: Correlative microscopy, Ferroelastic transformation, Nanotwins, transmission Kikuchi diffraction, atom probe tomography.

*Author for correspondence: Dr.-Ing. K. G. Pradeep

Contact number: +91 44 2257 4764

E-mail: kgprad@iitm.ac.in

Permanent address:
Department of Metallurgical and Materials Engineering,
Indian Institute of Technology Madras, Chennai – 600036, India.

$YTaO_4$ (YT) based materials have attracted attention owing to their high temperature phase stability and for their similarity with the yttria-zirconia system [1]. The thermal conductivity of sintered YT has been reported to be ~1.5 W m^{-1} K^{-1} at 800 °C which is 30% lesser than that of the currently successful 8 Yttria Stabilized Zirconia (YSZ) Thermal Barrier Coating (TBC) [2], [3]. As limited phase stability restricts the usage of 8 YSZ in the next generation gas turbine engines with an inlet temperature of 1482 °C, new TBC materials are being explored [4], [5]. Owing to the low thermal conductivity at high temperatures, ferro-elastic transformation assisted toughening, high thermal expansion coefficient (~10^{-5} K^{-1} at 1200 °C), and relatively low Young's modulus (~138 GPa), YT based materials are promising for next generation TBC applications [4], [6]. It has been reported that YT exhibits two monoclinic (M and M') and two tetragonal (T and T') phases [7], [8]. While, the M' (monoclinic, space group: P2/a) phase has been described as a thermodynamically stable phase, it can undergo a reconstructive transformation to the metastable T phase (tetragonal, space group: $I4_1/a$) at ~ 1450 °C [7]. In terms of structure, T and M phases (monoclinic, space group: I2) are closely related [7]. For instance, upon cooling, the T phase undergoes a second order ferro-elastic transformation to M phase (monoclinic, space group: I2) at 1426 ± 7 °C [7]. Besides, there is a very small difference (~-0.121 $kJmol^{-1}$) in terms of Gibbs free energy for M and M' phases [7]. Mather and Davies [8] have reported the possibility of T' phase (tetragonal, space group: $P4_2/nmc$) formation on annealing between 700-850 °C in YT materials synthesized using chemical processing techniques. In addition, T' has been described as a tetragonal distorted form of cubic fluorite with a random distribution of cations [8]. For 10 mol.% ZrO_2 added YT (10ZYT), the stabilized M phase has been reported to show two twin domain variants (angle between the variants being ~95.05°) along with retained T phase after annealing at 1500 °C for 5 h [9]. This indicates that the ferro-elastic T to M transformation can be incomplete even after annealing at 1500 °C for 5h [9]. However, the reason for the evolution of two twin domain variants in M phase is not fully understood. Besides, the stabilization of high temperature T phase with minor addition (<5 mol.%) of ZrO_2 at room temperature has not been explored so far.

Correlative microscopy, on the other hand has emerged as a powerful technique for the characterisation of nanoscale features, providing structural as well as chemical information from the same region of interest [10]–[13]. To this end, comprehensive microstructure analysis and chemical homogeneity of the ZYT system as a function of ZrO_2 content has not been reported. Hence, the present work intends to utilize custom-developed correlative microcopy

approach towards comprehensive investigation of nano-twinned domains including the orientation relationship, misorientation between the twin domains and their chemical homogeneity in 2 mol.% ZrO_2 alloyed YT (2ZYT). In addition, the stability of T phase and their possible retention at room temperature with minor (2 mol.%) addition of ZrO_2 is investigated both experimentally as well as by Ab-initio calculations.

Reverse co-precipitation technique was employed to prepare 2ZYT powders as per the procedures described in [1], [9], [14]. Zirconium dichloride oxide hydrate (Alfa Aesar, 99.9% purity), yttrium (III) nitrate hexahydrate and tantalum (V) chloride (both Sigma Aldrich, 99.8% purity) were used as starting materials. Sintering was caried out at 1485 °C for 3 h (heating and cooling rate was 5 °C min^{-1}).

X-ray diffraction (XRD) was performed on the sintered pellet using Co K_α radiation (λ= 0.179 nm) in Bruker D8 General Area Detector Diffraction System. Rietveld refinement was performed (using FullProf Suite Software) for the determination of lattice parameters in the phases present [15]–[17]. Raman spectroscopy was carried out at room temperature on sintered 2ZYT bulk samples using a confocal Raman system (Wi-Tech, alpha 300 M+) with 532 nm laser beam and spot size < 1 µm.

Correlative microscopy analysis was performed using Scanning Electron Microscope (SEM) - based techniques namely, Scanning Transmission Electron Microscopy (STEM), Energy Dispersive X-ray Spectroscopy (EDS) and Transmission Kikuchi Diffraction (TKD). A custom-designed holder capable of handling half-cut, 3 mm diameter Transmission Electron Microscope (TEM) grids was utilized. The holder facilitates Focussed Ion Beam (FIB)-based site-specific preparation of electron transparent lamella. Sample preparation for correlative SEM-STEM imaging, EDS and TKD mapping was performed using a dual-beam system, Thermofisher Helios Nanolab G4 UX [13]. TKD data analysis was performed using TSL OIM v8 software. Elemental distribution at near-atomic scale and chemical composition analysis was performed using Local Electrode Atom Probe, 5000X HR. Atom Probe Tomography (APT) measurements were performed with the sample tip maintained at 60 K. Data reconstruction and analysis was performed using IVAS 3.8.4 software provided by Cameca instruments.

Ab-initio calculations were performed to understand phase formation and stability in YT and 2ZYT. The first-principle calculations were performed using a plane-wave basis set as implemented in VASP (Vienna Ab initio Simulation Package) to predict the lattice parameters

of M and T phases. Projected Augmented Wave (PAW) method was used to describe the ion-electron interaction. The calculations were performed using a supercell consisting of 16 YT units. Stopping criteria for electronic self-consistent loop was chosen to be 10^{-6} eV, and the structural relaxation was stopped with the criterion of 10^{-5} eV/Å. Conjugate gradient algorithm was used to update the position of ions for M and T. All the structural degrees of freedom were allowed to change for the M phase, whereas only atomic positions were allowed to change for T phase.

Microstructural characterisation of 2ZYT was performed correlatively using high resolution SEM-based STEM and TKD techniques. Fig. 1(a, b) shows SEM chamber view and the schematic of in-house developed correlative microscopy holder with the pre-tilt arrangement facilitating both STEM analysis and unhindered TKD measurement. Fig. 1(c) shows SEM-STEM image along the cross section of the lamella in custom annular mode. Three grains with uniform distribution of refined single nanodomains are visible, which at higher magnification (inset) resembles the nano twins and their boundaries marked by dotted lines (in red). Fig. 1(d) shows the corresponding TKD-based inverse pole figure (IPF) map, which reveals the orientations of the nano twinned domains. Phase distribution map suggests the presence of alternate domains of T and M phases (with volume fractions: 0.49 and 0.51 respectively) within the same grain as shown in Fig. 1(e). The estimated misorientation angle across the nanotwins (blue line in Fig. 1(e)) was approximately 90° (Fig. 1(f)). From the pole figures of M and T phases (Fig. 1(g, h)), the prevalent orientation relationship between M and T phases with $[100]_M$ II $[001]_T$; $[010]_M$ II $[100]_T/[010]_T$ is apparent. In the context of m-ZrO_2, Bingham et al. [18] and Gertsman et al. [19] reported the presence of Σ6 near coincidence site lattice (CSL) GB with a misorientation angle of nearly 90°. In addition, transformation twins in m-ZrO_2 can be denoted as Σ3a 90.81° [100] and Σ3b 90.81° [001] CSL GBs [19]. Besides, the structure of Σ3a and Σ3b GBs may be considered to be equivalent to those of Σ71a and Σ71b, respectively [20]. For the case of ZYT, Shian et al. [9] have reported the presence of transformation twins with a or the case of YT, Shian et al. [9] have reported the presence of transformation twins with a misorientation angle ~95.50° between (2 0 -9.1) and (9.1 0 2) planes in M phase. In the present work with 2ZYT, the misorientation angle between the single nano-twinned domains (i.e. M and T phases) have been observed to be ~90°. Hence, it could be considered that these nanotwin boundaries can be highly stable owing to their low energy configuration.

Fig. 2(a) shows the room temperature XRD pattern of the 2ZYT sintered pellet. Most of the M and T phase peaks are observed to overlap with each other (Fig. 2(a)). Rietveld refinement confirms the presence of two phases namely, M and T in-line with the observations of TKD. The Goodness-of-fit parameter, χ^2 value was 1.03 considering the presence of both M and T phases indicating a reasonable fit, compared to an ideal case scenario where χ^2 value is expected to be around one [21]. It has to be noted that when refinement is carried out on powder samples or single crystals with simple crystal structures (or of high symmetry), χ^2 value of less than one is generally achieved [9], [22]. In the case of polycrystalline materials with complex (or low symmetry) crystal structures as in the present case, the values for the fitting parameters can be expected to be more than one [15], [16], [23].

To further support the observations of TKD and XRD, Raman spectroscopy was performed. Fig. 2(b) shows the Raman spectra of 2ZYT at room temperature which reveals the presence of both M & T phases, with the highest peaks of M and T at 327 and 302 cm^{-1} respectively (Fig. 2(b)). The Raman peaks obtained for M phase (Fig. 2(b)) are in good agreement with the reported peaks of M phase [6], [24], [25]. The presence of retained T phase at room temperature (Fig. 2(b)) can be confirmed from the appearance of three distinct peaks (302, 628 and 744 cm^{-1}) closely resembling the simulated peak positions (309, 625 and 749 cm^{-1}) [6]. The relative peak intensities for M and T phases suggest that M is the majority phase. Recently, Stelzer et al. [7], had observed the evolution of M phase in YT system with ZrO_2 content ≥11 mol.% in a reactively sputtered ZYT coatings and attributed the formation of T phase to local distortions caused due to the substitution of Zr to Ta^{5+} and larger Y^{3+} cations.

Fig. 3 presents the 3D elemental distribution map obtained from APT. All the constituent elements are distributed homogeneously without apparent indication of clustering or presence of Y_3TaO_7, YTa_7O_{19}, $Zr_6Ta_2O_{17}$ or $Y_4Zr_3O_{12}$ precipitates (which have been reported to be thermodynamically stable in these systems [26]–[28]–[28]–[28]–[28]–[The 1D concentration profile obtained along the 5 nm diameter cylindrical region of interest indicates the near stoichiometric concentration of elements as expected in this system [7]. . For comparison, a wide area elemental mapping inclusive of multiple twin domains as well as a grain boundary was performed using correlative SEM-EDS during TKD measurement. The uniform distribution of all elements across the grain boundary and nano twin domains can be confirmed (supplementary Fig. S2). Besides, the composition obtained from APT analysis of the grain boundary region (supplementary Fig. S3) is highly consistent with the bulk composition obtained using SEM-EDS (supplementary Table. S1).

Fig. 4 shows the variation in the relative stability of M, M', T and T' phases as a function of ZrO_2 alloying. It is observed that M' (difference between M' and T' ground state energies (ΔE) being negative) is the most stable phase amongst all the considered phases. Similar observations of M' to be the most stable phase at 0 K was reported in Ref. [29]. However, the propensity of stabilizing both M and T phases (ΔE close to 0 for M-T) are noticeable irrespective of ZrO_2 alloying. Based on these observations, there exists a strong possibility for the co-existence of M and T phases at room temperature especially for 2 mol.% ZrO_2 addition when the system is subjected to second order displacive phase transformation. Therefore, the observations based on ab-initio calculations are in good agreement with the experimental results of correlative microscopy, XRD and Raman spectroscopy (Fig. 2) as well as the other reports [7] [30]. The comparative lattice parameters of both M and T phases after Rietveld refinement and ab-initio calculations are presented in Table. 1, which are also in good agreement with each other and with reported values [6], [9]27].

Table 1. A comparison of the lattice parameters and angles for both M and T phases determined using XRD (after Rietveld refinement) and ab-initio calculations for 2ZYT.

	Experimental (XRD - Rietveld)		**Theoretical (Ab-initio calculations)**	
Cell parameters	**M phase**	**T phase**	**M phase**	**T phase**
a (Å)	5.23	5.26	5.34	5.21
b (Å)	10.93	5.26	11.03	5.21
c (Å)	5.06	11.26	5.09	11.00
α (°)	90	90	90	90
β (°)	95.26	90	95.53	90
ɤ (°)	90	90	90	90

Ferro-elastic transformations also described as second order phase transformations [9], involve spontaneous strain which has been described as the measure of the degree of ferro-elasticity and is required to account for lattice distortions associated with it [31]. In the present work, T to M ferro-elastic phase transformation of 2ZYT occurs when the temperature is decreased

below the T-M transformation temperature (~1426 ± 7° [6]). The system forms two equivalent domain states (S1 and S2) in the monoclinic phase of YT [6]. Though the domains have the same free energy, they differ in their orientation states and hence have different strain tensors [6]. The magnitude of the spontaneous strain, $(\varepsilon_s)^2$ is given by, [31]

$$(\varepsilon_s)^2 = 2\,[(\varepsilon^s_{ij}(S1))^2 + (\varepsilon^s_{ij}(S2))^2] \qquad (1)$$

where, $\varepsilon^s_{ij}(S1)$ is the strain tensor due to S1

$\varepsilon^s_{ij}(S2)$ is the strain tensor due to S2

Spontaneous strain calculations (using eq. 1) are based on crystal symmetries. For such transformations in 2ZYT, it can be assumed that $(\varepsilon_s)^2 = 0$ in the parent *T* phase, similar to those reported elsewhere [9]. In addition, only one domain state has been observed in STEM-TKD (Fig. 1). Hence, $\varepsilon^s_{ij}(S2)$ becomes zero. This implies that $(\varepsilon_s)^2$ generated in the material under study (sintered at 1485 °C for 3 h) has to be lower than that of YT (sintered at 1500 °C for 5 h) or that of the extrapolated 2ZYT material [9]. Alloying of lanthanum orthoniobate ($LaNbO_4$) (which is iso-structural to ZrO_2 alloyed YT [9]) with antimony (Sb), has been reported to decrease both the *T-M* transition temperature and $(\varepsilon_s)^2$ when compared with that for the unsubstituted material viz. $LaNbO_4$ [32], [33].

Further to rationalize the T phase stability and observed lattice parameter, the T form of $YNbO_4$ having a distorted scheelite ($CaWO_4$) structure can be used for comparison. Similar to Y^{3+} and Nb^{5+} ions in both M and T forms of $YNbO_4$, Y^{3+} and Ta^{5+} ions (in M and T phases of YT) prefer eight-fold and four-fold coordination respectively [9]. On the other hand, Zr has only 4+ charge state and the coordination number may vary between 4 to 9 [34]. In ZrO_2, Zr^{4+} prefers an eight-fold or a seven-fold coordination [35]. On adding ZrO_2 to YT, it has been reported that a pair of Zr^{4+} ions substitute for Y^{3+} and Ta^{5+} ions in the unit cell wherein charge neutrality is maintained without any oxygen vacancy formation [9]. In addition, the ionic radii of Y^{3+}, Zr^{4+} and Ta^{5+} are 0.1019, 0.084 and 0.074 nm respectively [9]. A comparison of the mean ionic radii of Y^{3+} and Ta^{5+} (~0.087 nm) with the ionic radius of Zr^{4+} (~0.084 nm) suggests that the substitution of both Y^{3+} and Ta^{5+} by Zr^{4+} leads to a slight distortion in the T crystal structure of YT phase and a subsequent decrease in unit cell volume of T-YT phase. Consequently, a considerable difference in the unit cell volumes of the T phase of YT is expected with increase in ZrO_2 addition.

To summarize, the experimental results obtained using correlative SEM-TKD, XRD and Raman spectroscopy techniques supported by ab-initio calculations reveal the co-existence of two phases (T and M) in 2ZYT synthesized using reverse co-precipitation method. The key conclusions are summarized as,

1. The characteristic feature of ferro-elastic transformation i.e. the formation of nano-twinned domains has been presented with an average domain spacing of 154.07 ± 42.52 nm, where $[100]_M \parallel [001]_T$; $[010]_M \parallel [100]_T/[010]_T$, while maintaining a constant misorientation angle of 90°.
2. The uniform distribution of constituent elements across M and T phases has been correlated using the combined TKD-APT approach.
3. The retention of T phase at room temperature coupled with spontaneous strain calculations (based on crystal symmetries) for the observed single domain configuration collectively suggest the metastable state of 2ZYT sintered at 1485 °C for 3 hr.

Hence, the possibility of retaining the high temperature T phase at room temperature within a single domain structure by ZrO_2 alloying has been established which allows for future exploration of novel, highly stable ZYT based TBC material.

Declaration of competing interest

The authors declare that they have no known competing financial interests or personal relationships that could have appeared to influence the work reported in this paper.

Acknowledgement

The authors would like to thank National Facility for Atom Probe Tomography at IIT Madras for APT measurements. KGP acknowledges the funding support of Max-Planck Gesellschaft for establishing Max-Planck-India Partner group at IIT Madras. MBP thanks Srinivas Reddy for support with sample preparation. KGP is also grateful for the funding support from IIT Madras under Exploratory Research Project to carry out this work. KGP also acknowledges the funding support from Ministry of Human Resource and Development through the Institute of Eminence (IoE) initiative for establishing the Center of Excellence in Correlative Microscopy.

References

[1] S. Raghavan, H. Wang, R.B. Dinwiddie, W.D. Porter, R. Vaβen, D. Stöver and M.J. Mayo, *Journal of the American Ceramic Society*, 87 (2004) 431–437.

[2] J. Wang, Y. Zhou, X. Y. Chong, R. Zhou, and J. Feng, *Ceramics International*, 42 (2016) 13876–13881.

[3] A. M. Limarga, S. Shian, R. M. Leckie, C. G. Levi, and D. R. Clarke, *Journal of the European Ceramic Society*, 34 (2014) 3085–3094.

[4] L. Chen, M. Hu, P. Wu, and J. Feng, *Journal of the American Ceramic Society*, 102 (2019) 4809–4821.

[5] M. Hayakawa and M. Oka, *Acta Metallurgica*, 37 (1989) 2229–2235.

[6] J. Feng, S. Shian, B. Xiao, and D. R. Clarke, *Physical Review B - Condensed Matter and Materials Physics*, 90 (2014) 094102.

[7] B. Stelzer *et al.*, *Materials*, 14 (2021) 1–15.

[8] S. A. Mather and P. K. Davies, *Journal of the American Ceramic Society*, 78 (1995) 2737–2745.

[9] S. Shian, P. Sarin, M. Gurak, M. Baram, W. M. Kriven, and D. R. Clarke, *Acta Materialia*, 69 (2014) 196–202.

[10] Y. J. Li, A. Kostka, A. Savan, and A. Ludwig, *Scripta Materialia*, 183 (2020) 122–126.

[11] P. W. Trimby *et al.*, *Acta Materialia*, 62 (2014) 69–80.

[12] T. Schwarz, G. Stechmann, B. Gault, O. Cojocaru-Mirédin, R. Wuerz, and D. Raabe, *Progress in Photovoltaics: Research and Applications*, 26 (2018) 196–204.

[13] K. G. Pradeep, K. Chang, A. Kovács, S. Sen, A. Marshal, René de Kloe, R. E. Dunin-Borkowski and J. M. Schneider, *Materials Research Letters*, 7 (2019) 180–187.

[14] M. Gurak, Q. Flamant, L. Laversenne, and D. R. Clarke, *Journal of the European Ceramic Society*, 38 (2018) 3317–3324.

[15] H. M. Rietveld, *Journal of Applied Crystallography*, 2 (1969) 65–71.

[16] H. M. Rietveld, *Acta Crystallographica*, 22 (1967) 151–152.

[17] J. Rodriguez-Carvajal, Refinement of Crystal and Magnetic Structures from Powder and Single Crystal Data.

[18] D. Bingham, P. W. Tasker, and A. N. Cormack, *Philosophical Magazine A: Physics of Condensed Matter, Structure, Defects and Mechanical Properties*, 60 (1989) 1–14.

[19] V. Y. Gertsman, A. P. Zhilyaev, and J. A. Szpunar, *Modelling and Simulation in Materials Science and Engineering*, 5 (1997) 35–52.

[20] H. Grimmer, *Acta Crystallographica Section A*, 32(1976) 783–785.

[21] S. M. Patange, S. E. Shirsath, G. S. Jangam, K. S. Lohar, S. S. Jadhav, and K. M. Jadhav, *Journal of Applied Physics*, 109 (2011) 53909.

[22] G. M. Wolten, *Acta Crystallographica*, 23 (1967) 939–944.

[23] M. B. Ponnuchamy and A. S. Gandhi, *Scripta Materialia*, 83 (2014). 21–24.

[24] Q. Flamant, M. Gurak, and D. R. Clarke, *Journal of the European Ceramic Society*, 38 (2018) 3925–3931.

[25] F. M. Pitek and C. G. Levi, *Surface and Coatings Technology*, 201 (2007) 6044–6050.

[26] C. A. Macauley, A. N. Fernandez, and C. G. Levi, *Journal of the European Ceramic Society*, 37 (2017) 4888–4901.

[27] A.N. Fernandez, C.A. Macauley, D. Park, and C.G. Levi, *Journal of the European Ceramic Society*, 38 (2018) 4786–4798.

[28] S. Shukla and S. Seal, *International Materials Reviews*, 50 (2005) 45–64.

[29] F. Zhang, G. Zhang, L. Yang, Y. Zhou, and Y. Du, *Journal of the European Ceramic Society*, 39 (2019) 5036–5047.

[30] S. G. Heinze, A. R. Natarajan, C. G. Levi, and A. van der Ven, *Physical Review Materials*, 2 (2018) 073607.

[31] K. Aizu, *Journal of the Physical Society of Japan*, 28 (1970) 706–716.

[32] S. Wachowski, A. Mielewczyk-Gryn, and M. Gazda, *Journal of Solid State Chemistry*, 219 (2014) 201–209

[33] A. Mielewczyk-Gryn, S. Wachowski, K. I. Lilova, X. Guo, M. Gazda, and A. Navrotsky, *Ceramics International*, 41 (2015) 2128–2133.

[34] R. D. Shannon, *Acta Crystallographica Section A*, 32 (1976) 751–767.

[35] A. H. Heuer, Journal *of the American Ceramic Society*, 70 (1976) 689–698.

Figure Captions:

Fig. 1 (a) SEM chamber view, (b) schematic illustration of custom designed correlative microscopy holder suitable for STEM imaging, EDS mapping and TKD analysis. The microstructure of the 2ZYT sample obtained from the electron transparent region. (c) SEM based STEM image (in custom annular mode); TKD-based (d) Inverse pole figure map and (e) phase distribution maps. (f) Plot showing misorientation angle (in degrees) across nano-twins and the average thickness of nano-twins. Both misorientation angle and average twin thickness in (f) have been determined along the blue line in (e)**.** Pole figures for (g) Monoclinic (M) and (h) Tetragonal (T) phases generated from the enclosed rectangle region (violet) in (d) and (e).

Fig. 2 (a) Rietveld refined XRD pattern, and (b) Raman spectra showing the presence of M and T phases in 2ZYT at room temperature.

Fig. 3 Three-dimensional elemental distribution maps of Y (pale blue), Ta (maroon), O (sky blue) and Zr (violet) from 2ZYT and 1D concentration profile obtained along the 5 nm diameter cylindrical region of interest showing homogeneous distribution of the elements.

Fig. 4 Variation of the relative stability (ΔE in eV) of M, M', T and T' phases as a function of ZrO_2 content. The inset images above ΔE=0 (red dotted line) indicate the atomic positions of Y, Ta, Zr and O atoms in T phase (along a-b and a-c planes). Similarly, the inset images below

ΔE=0 indicate the atomic positions of constituent elements in M phase (along a-b and a-c planes).

Graphical Abstract

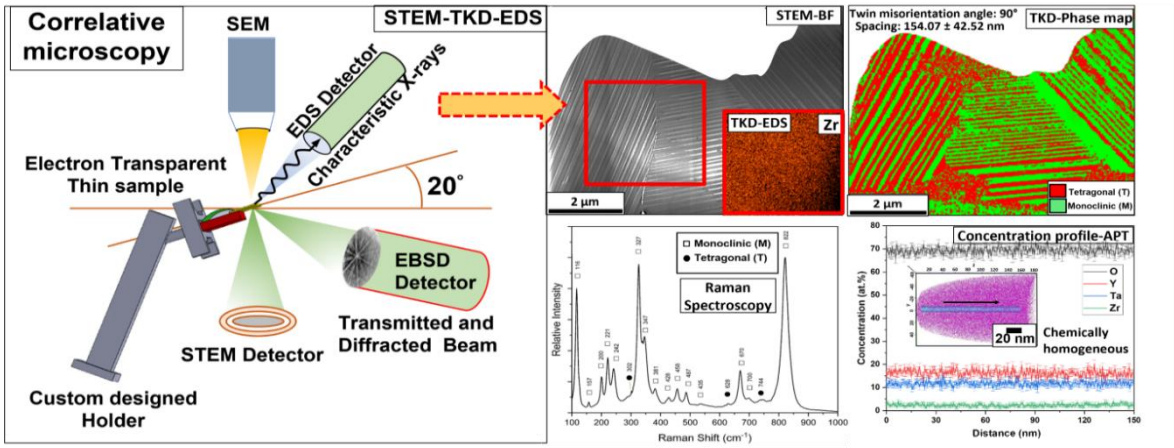

Supplementary data

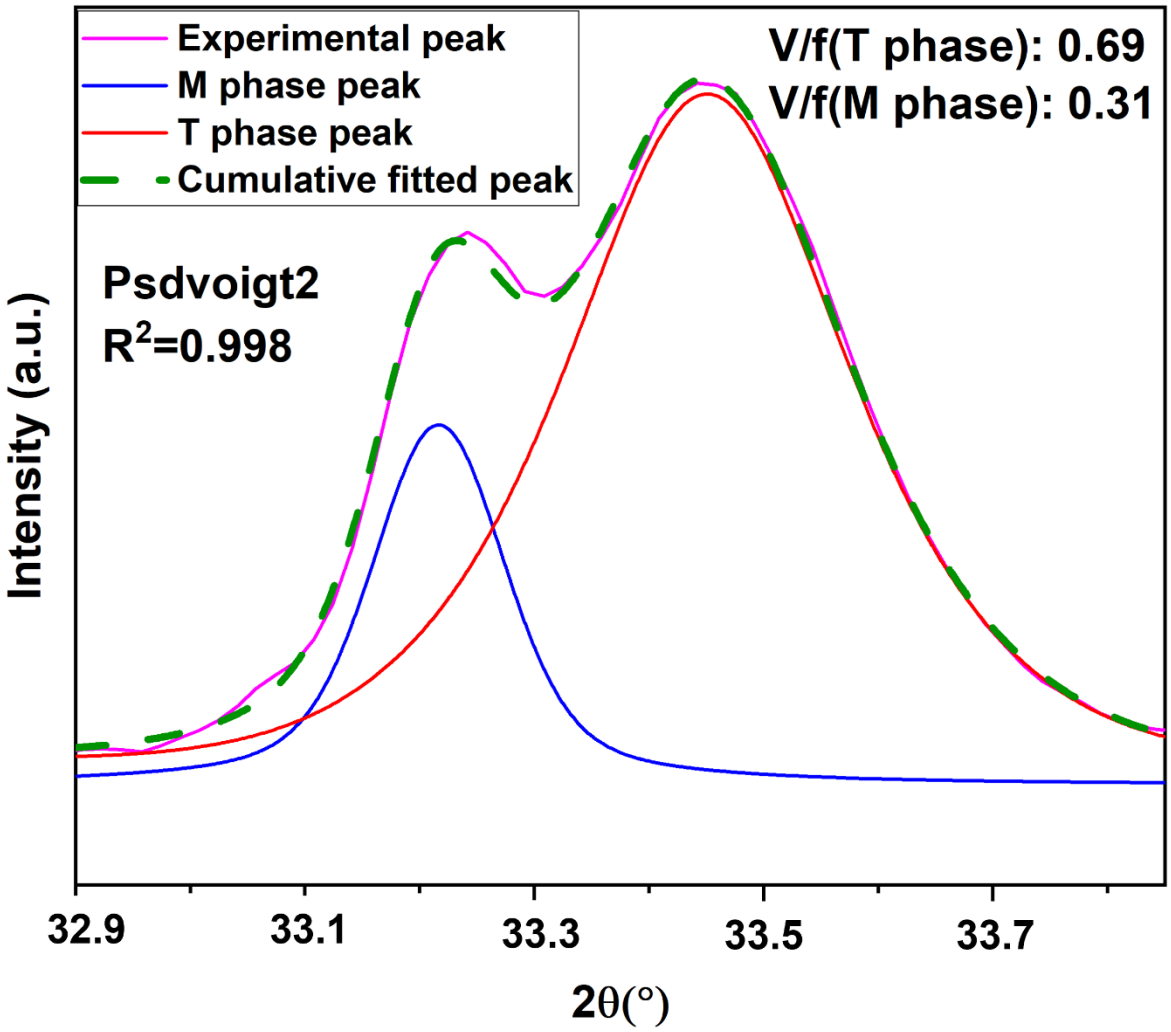

Fig. S1 XRD: Deconvolution of the highest intensity peaks of M and T phases respectively in 2ZYT.

Most of the peaks belonging to M and T phases are observed to overlap with each other in the XRD pattern of 2ZYT (as shown in Fig. 2(a) in the manuscript). Hence, a deconvolution of the highest intensity peaks of M and T phases respectively (in 2ZYT) has been performed for the purpose of determining the volume fraction of M and T phases.

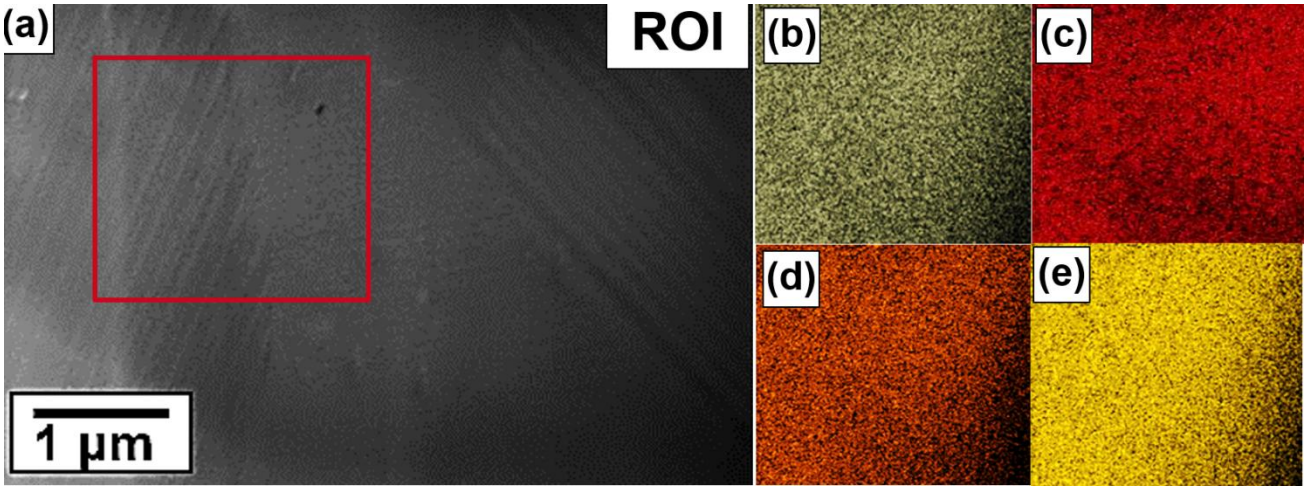

Fig. S2 2ZYT: **(a)** STEM image, TKD-Energy Dispersive Spectroscopy (EDS) maps of: **(b)** Y, **(c)** Ta, **(d)** Zr, and **(e)** O showing a uniform elemental distribution among the nano-twinned domains in both M and T phases. The EDS maps in parts **(b-e)** have been obtained from the region enclosed within the red-outlined square in part **(a).**Correlative STEM-EDS mapping was performed across the grain boundary region with the inclusion of at least 10 nano-twinned domains (indicated by square in Fig. S2 (a)) to understand the elemental distribution across the interface region **(Fig. S3).** The qualitative elemental mapping indicated the uniform distribution of constituent elements as can be seen in Fig. S21 (b-e). Considering that quantification of elemental concentration by EDS especially for elements such as Oxygen are not reliable, atom probe tomography measurement was performed for the precise determination of composition as well as the three-dimensional elemental distribution.

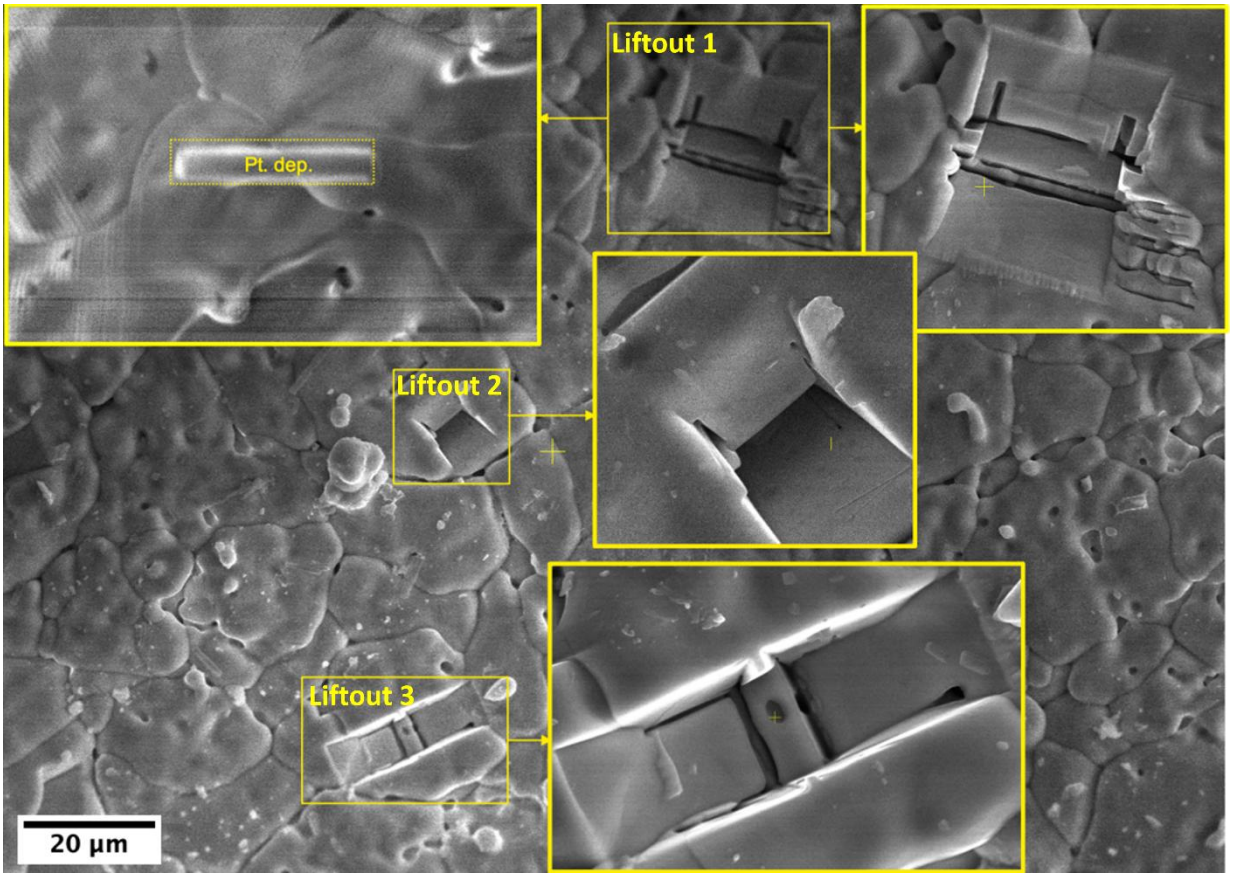

Fig. S3 2ZYT: SEM image of the interface region from where APT needles were prepared. Yellow-outlined rectangles enclose the Pt-deposited region from where FIB liftout for APT was performed.

Table. S1 Bulk composition based on SEM-EDS mapping

Element	At.%
Y	**16.6 ± 1.72**
O	**64.1 ± 7.44**
Ta	**16.9 ± 0.59**
Zr	**2.4 ± 0.49**

Comparing the APT results (Fig. 3 in the main manuscript) with the bulk composition obtained using SEM-EDS (Table. S1), a consistency may be observed in terms of Y, O, Ta and Zr contents.

Fig. S4

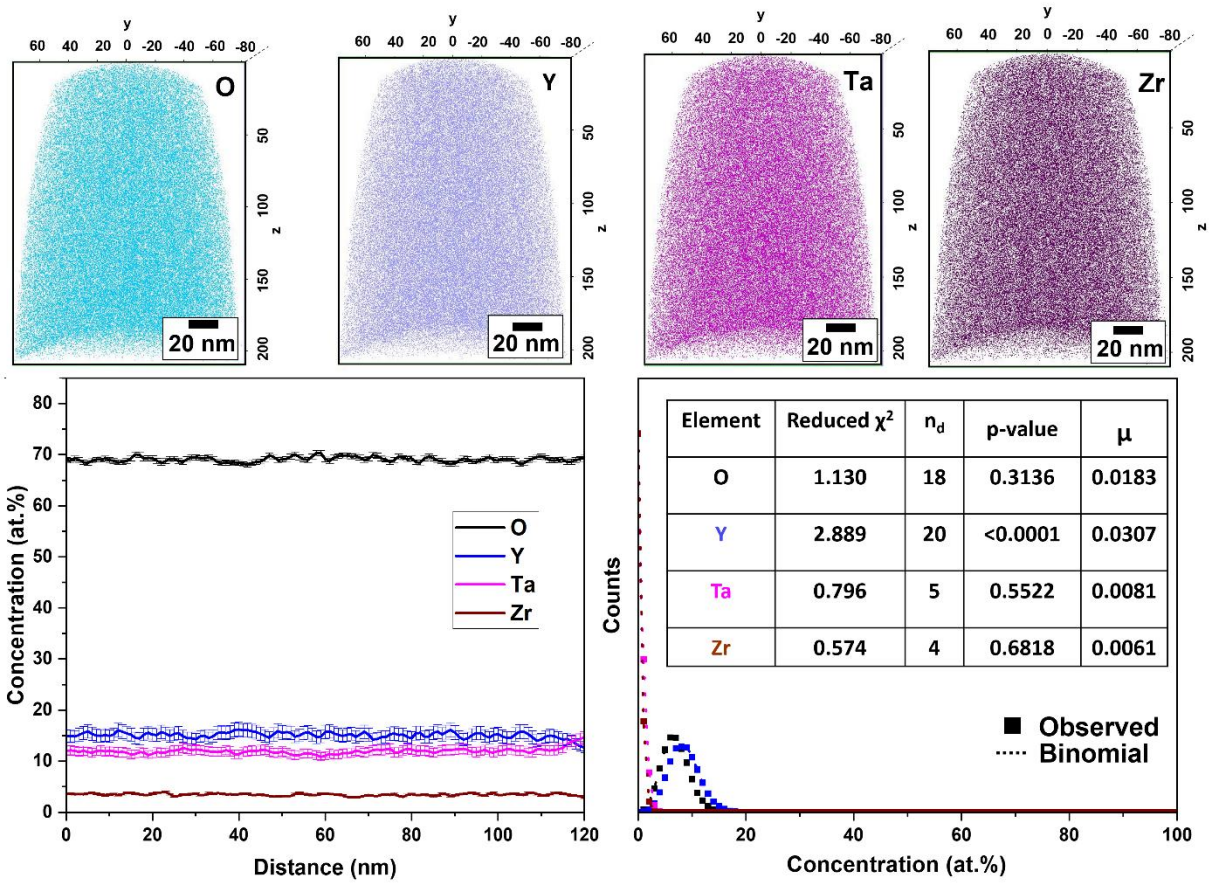

Element	Reduced χ^2	n_d	p-value	μ
O	1.130	18	0.3136	0.0183
Y	2.889	20	<0.0001	0.0307
Ta	0.796	5	0.5522	0.0081
Zr	0.574	4	0.6818	0.0061